Quantum computing of the pairing Hamiltonian at finite temperature

Chongji Jiang[1] and Junchen Pei[1,2,*]

[1]*State Key Laboratory of Nuclear Physics and Technology, School of Physics, Peking University, Beijing 100871, China*

[2]*Southern Center for Nuclear-Science Theory (SCNT), Institute of Modern Physics, Chinese Academy of Sciences, Huizhou 516000, China*

(Received 16 December 2022; revised 10 March 2023; accepted 23 March 2023; published 14 April 2023)

In this work, we study the pairing Hamiltonian with four particles at finite temperatures on a quantum simulator and a superconducting quantum computer. The excited states are obtained by the variational quantum deflation. The error-mitigation methods are applied to improve the noisy results. The simulation of thermal excitation states is performed using the same variational circuit as at zero temperature. The results from quantum computing become close to exact solutions at high temperatures, and demonstrate a smooth superfluid-normal phase transition as a function of temperatures as expected in finite systems.

DOI: 10.1103/PhysRevC.107.044308

I. INTRODUCTION

The simulation of quantum many-body systems on quantum computers has natural advantages by avoiding the exponential scaling of computing costs on classical computers [1]. Atomic nuclei are strongly correlated finite quantum many-body systems, for which the accurate treatment of many-body correlations is essential. There are already several applications of quantum computing in nuclear physics, such as the implementation of coupled cluster method for light nuclei [2], the Lipkin model [3,4], neutrino-nucleus scattering [5], nuclear dynamics [6,7], the symmetry restoration [8], and the nuclear shell model [9] on quantum computers. Presently these applications in simplified many-body models paved a route to practical quantum computing of small quantum systems such as light nuclei in the near future.

Actually small quantum systems have novel features compared to large systems. For large systems the statistical methods or mean-field theories are often suitable theoretical tools. In particular, there is a superfluid-normal phase transition in large systems with increasing temperatures but the phase transition is absent in finite small systems. In this respect, the finite-temperature Bardeen–Cooper–Schrieffer (BCS) or Hartree-Fock-Bogoliubov theory is breakdown which results in a false pairing phase transition in nuclei [10]. With elaborate many-body approaches, such as the quantum Monte Carlo [11] and particle number projections at finite temperatures [12], the false phase transition is washed out. In addition, the existence of a pseudogap phase in high-T_c superconductors has been widely studied and the origin of the pseudogap remains an open question [13,14]. Indeed, the exact treatment of thermal excitations of quantum systems has broad implications in static and dynamical observables. The accurate descriptions of hot nuclei and nuclear matter are relevant for descriptions of level densities [15], shape transitions [11,16], fission barriers [17], and equation of state for neutron stars [18].

There are several quantum algorithms to simulate many-body systems on quantum computers. The widely used variational quantum eigensolver (VQE) is a robust and flexible way to compute the ground state of a Hamiltonian [2,19]. The modified VQE, namely variational quantum deflation (VQD), can be applied to excited states [20]. In addition, the quantum phase estimation method can also solve the eigenstate problems which requires deep circuits with ancilla qubits [8]. On the other hand, the hybrid quantum and classical computing has been extensively studied so that the optimization of VQE is feasible [21]. Besides quantum algorithms, the development of quantum computing hardware is fast and IBM is expected to deliver a 4000-qubit system by 2025.

In this work, the ground state, excited states, and thermal states of the pairing Hamiltonian are studied with the variational quantum computation. One of the key issues is to apply VQD to solve excited states and their degeneracies. Although the quantum computing of the pairing Hamiltonian and the Lipkin model have been studied in the literatures [3,4,8], a comprehensive study of eigenstates and thermal states is still inspiring. The finite-temperature BCS results with a false phase transition are also shown for comparison to emphasize the significance of quantum computing. The calculations are firstly performed with the simulator Qiskit [22]. Then practical quantum computing is performed on a superconducting quantum computer provided by IBM. The error mitigation methods for the noisy quantum computing have also been discussed.

II. THEORETICAL FRAMEWORK

This work solves the pairing Hamiltonian in a degenerate shell space, which has exact solutions for benchmark of different methods. It is known that the fermionic operators can be implemented on quantum computers with the Jordan-Wigner transformation [2,8,23,24]. For the pairing Hamiltonian, it is

*peij@pku.edu.cn

TABLE I. The exact solution in the qubit basis space for the pairing Hamiltonian with $N = 4$ particles in a degenerate shell space of $\Omega = 3$ and $\Omega = 4$. In the table, S_0 denotes the z component of the total spin and s denotes the seniority number based on the seniority model.

(Ω, N)	S_0	Basis	Eigenstates	s	Eigenvalue
(3,4)	$\frac{1}{2}$	$\|\uparrow\uparrow\downarrow\rangle, \|\uparrow\downarrow\uparrow\rangle, \|\downarrow\uparrow\uparrow\rangle$	$\frac{1}{\sqrt{3}}(\|\uparrow\uparrow\downarrow\rangle + \|\uparrow\downarrow\uparrow\rangle + \|\downarrow\uparrow\uparrow\rangle)$	0	$-4G$
			$\frac{1}{\sqrt{2}}(\|\uparrow\uparrow\downarrow\rangle - \|\uparrow\downarrow\uparrow\rangle)$ $\frac{1}{\sqrt{6}}(-\|\uparrow\uparrow\downarrow\rangle - \|\uparrow\downarrow\uparrow\rangle + 2\|\downarrow\uparrow\uparrow\rangle)$	2	$-G$
(4,4)	0	$\|\uparrow\downarrow\downarrow\uparrow\rangle, \|\downarrow\uparrow\downarrow\uparrow\rangle, \|\downarrow\downarrow\uparrow\uparrow\rangle,$ $\|\uparrow\uparrow\downarrow\downarrow\rangle, \|\uparrow\downarrow\uparrow\downarrow\rangle, \|\downarrow\uparrow\uparrow\downarrow\rangle$	$\frac{1}{\sqrt{6}}(\|\uparrow\uparrow\downarrow\downarrow\rangle + \|\uparrow\downarrow\uparrow\downarrow\rangle + \|\downarrow\uparrow\uparrow\downarrow\rangle +$ $\|\uparrow\downarrow\downarrow\uparrow\rangle + \|\downarrow\uparrow\downarrow\uparrow\rangle + \|\downarrow\downarrow\uparrow\uparrow\rangle)$	0	$-6G$
			$\frac{1}{\sqrt{2}}(\|\downarrow\uparrow\uparrow\downarrow\rangle - \|\uparrow\downarrow\downarrow\uparrow\rangle)$ $\frac{1}{\sqrt{2}}(\|\downarrow\downarrow\uparrow\uparrow\rangle - \|\uparrow\uparrow\downarrow\downarrow\rangle)$ $\frac{1}{\sqrt{2}}(\|\downarrow\uparrow\downarrow\uparrow\rangle - \|\uparrow\downarrow\uparrow\downarrow\rangle)$	2	$-2G$
			$\frac{1}{2}(\|\uparrow\downarrow\uparrow\downarrow\rangle - \|\downarrow\uparrow\uparrow\downarrow\rangle - \|\uparrow\downarrow\downarrow\uparrow\rangle +$ $\|\downarrow\uparrow\downarrow\uparrow\rangle)$ $\frac{\sqrt{3}}{3}(\|\uparrow\uparrow\downarrow\downarrow\rangle + \|\downarrow\downarrow\uparrow\uparrow\rangle) -$ $\frac{\sqrt{3}}{6}(\|\downarrow\uparrow\uparrow\downarrow\rangle + \|\uparrow\downarrow\downarrow\uparrow\rangle + \|\uparrow\downarrow\uparrow\downarrow\rangle +$ $\|\downarrow\uparrow\downarrow\uparrow\rangle)$	4	0

more efficient to map the pairs with the quasispin operators [25,26]. In this work, the pairing Hamiltonian is rewritten with the quasispin operators as [27]

$$H = -G \sum_{m,m'>0} a^+_{m'} a^+_{-m'} a_{-m} a_m = -G \sum_{m,m'>0} s^{(m')}_+ s^{(m)}_- \quad (1a)$$

with

$$s^{(m)}_+ = a^+_m a^+_{-m}, \quad s^{(m)}_- = a_{-m} a_m, \quad (1b)$$

where two orbitals of $(m, -m)$ form a pair. The quasispin operators s_+, s_- have the commutation properties of angular momentum operators.

It is convenient to map the transformed pairing Hamiltonian in the quasispin basis into qubit basis

$$H = -G \sum_{p,q>0} s^{(p)}_+ s^{(q)}_-, \quad (2a)$$

where the operators can be represented by Pauli matrices

$$s^{(p)}_+ s^{(p)}_- \to \tfrac{1}{2}\left(I^{(p)} + \sigma^{(p)}_z\right), \quad (2b)$$

$$s^{(p)}_+ s^{(q)}_- \to \tfrac{1}{2}\left(\sigma^{(p)}_x \otimes \sigma^{(q)}_x + \sigma^{(p)}_y \otimes \sigma^{(q)}_y\right). \quad (2c)$$

A. Details of the pairing Hamiltonian

In the following part, we describe the pairing Hamiltonian being mapped into the qubit basis. We study $N = 4$ particles in a $(2j + 1)$-fold degenerate j shell corresponding to $\Omega = 3$ and $\Omega = 4$, where $\Omega = j + \frac{1}{2}$ is the number of pairs. In the shell model, the configuration spaces for $\Omega = 3$ and $\Omega = 4$ are $C^4_6 = 15$ dimensional and $C^4_8 = 70$ dimensional, respectively. The complexity of classical computing increases exponentially with the shell space of Ω. The half-occupied configuration space leads to the largest computing costs. We will show that the pairing Hamiltonian can be simulated with three qubits for $\Omega = 3$ and with four qubits for $\Omega = 4$ and so on, which is irrespective of the number of particles.

For the case of $\Omega = 3$, the pairing Hamiltonian can be constructed on three qubits. The transformed pairing Hamiltonian is represented in terms of Pauli matrices according to Eq. (2). The pairing Hamiltonian of $\Omega = 3$ can be solved in the qubit basis space of $\{|\uparrow\uparrow\uparrow\rangle, |\uparrow\uparrow\downarrow\rangle, |\uparrow\downarrow\uparrow\rangle, |\uparrow\downarrow\downarrow\rangle, |\downarrow\uparrow\uparrow\rangle, |\downarrow\uparrow\downarrow\rangle, |\downarrow\downarrow\uparrow\rangle, |\downarrow\downarrow\downarrow\rangle\}$. For $N = 4$ and $\Omega = 3$, the eigenspace can be reduced to $\{|\uparrow\uparrow\downarrow\rangle, |\uparrow\downarrow\uparrow\rangle, |\downarrow\uparrow\uparrow\rangle\}$ since the number of particles is related to the z component of total spin. For $\Omega = 4$ and $N = 4$, the pairing Hamiltonian can be represented on four qubits in a reduced eigenspace of $(|\uparrow\uparrow\downarrow\downarrow\rangle, |\uparrow\downarrow\uparrow\downarrow\rangle, |\downarrow\uparrow\uparrow\downarrow\rangle, |\uparrow\downarrow\downarrow\uparrow\rangle, |\downarrow\uparrow\downarrow\uparrow\rangle, |\downarrow\downarrow\uparrow\uparrow\rangle)$. The exact solutions of the pairing Hamiltonian of $\Omega = 3$ and $\Omega = 4$ with four particles are given in Table I.

B. State preparation

Next we prepare the trial state on the quantum circuits. To simplify the quantum circuits, the symmetry of particle number conservation is exploited. For $\Omega = 3$ with $N = 4$ particles, the ansatz wave function with two variational parameters is represented as

$$|\psi\rangle_t = \sin\frac{\theta}{2}|\uparrow\uparrow\downarrow\rangle + \cos\frac{\theta}{2}\sin\eta|\uparrow\downarrow\uparrow\rangle + \cos\frac{\theta}{2}\cos\eta|\downarrow\uparrow\uparrow\rangle. \quad (3)$$

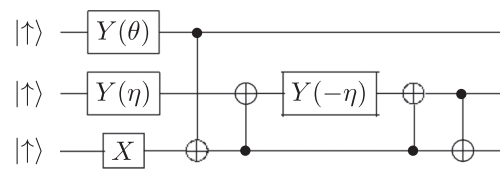

FIG. 1. Quantum variational circuit for $\Omega = 3$ and $N = 4$ on three qubits, in which the $Y(\theta)$ gate performs a rotation of θ around the Y-axis direction.

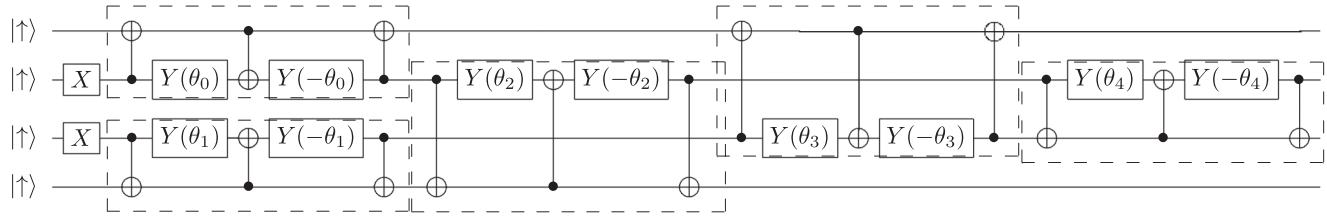

FIG. 2. Quantum variational circuit for $\Omega = 4$ and $N = 4$ on four qubits, which includes five two-qubit building blocks.

The quantum circuit of $\Omega = 3$ is shown in Fig. 1. The rotation angles η, θ correspond to the variational parameters.

For $\Omega = 4$ with four particles, the trial wave function in computational basis can be expressed by variational rotation angles $\theta_0, \ldots, \theta_4$. The associated quantum circuit with four qubits is shown in Fig. 2. For $\Omega = 4$ with six particles, the circuit can be much simpler with a reduced eigenspace. The circuit for $\Omega = 4$ is constructed according to the ansatz that preserves the number of particles, as presented in Refs. [28–30]. This circuit employs five two-qubit building blocks as shown in Fig. 2. Each building block $U(\theta)$ is written as

$$U(\theta) = \begin{pmatrix} 1 & 0 & 0 & 0 \\ 0 & \sin\theta & \cos\theta & 0 \\ 0 & \cos\theta & -\sin\theta & 0 \\ 0 & 0 & 0 & 1 \end{pmatrix}, \tag{4}$$

which is a unitary variational transformation but preserves the number of particles. In this way, the circuit is rather low-depth and results from quantum computing are less noisy. The circuits for systems with a larger Ω can also be constructed efficiently using the two-qubit building blocks.

C. VQD for excited states

First the ground state solution is obtained by adjusting the variational parameters in the Hamiltonian

$$E(\lambda) \equiv \langle\psi(\lambda)|H|\psi(\lambda)\rangle. \tag{5}$$

The ansatz state $|\psi(\lambda)\rangle$ is prepared with variational parameters λ, which are the rotation angles in quantum gates of the circuit. The ground state corresponds to the minimum energy by making measurements of Pauli terms of the pairing Hamiltonian. For circuits with multiple parameters, the optimized numerical method is needed to search the minimum.

VQD is a modification of VQE and can be applied to compute excited states [20]. For the kth excited state, the variational parameters λ_k for the ansatz state $\psi(\lambda_k)$ are obtained by minimizing the extended cost function as

$$E(\lambda_k) \equiv \langle\psi(\lambda_k)|H|\psi(\lambda_k)\rangle + \sum_{i=0}^{k-1} \beta_i |\langle\psi(\lambda_k)|\psi(\lambda_i)\rangle|^2. \tag{6}$$

This means that $\psi(\lambda_k)$ is required to be orthogonal to lower states. This is equivalent to solve an effective Hamiltonian $H(k)$ for kth excited states $|k\rangle$ as follows:

$$H(k) \equiv H + \sum_{j=0}^{k-1} \beta_j |j\rangle\langle j|. \tag{7}$$

Here, H represents the pairing Hamiltonian, $|0\rangle$ represents the ground state, and $|j\rangle$ represents jth excited state. The excited states are solved successively with increasing excitation energies. The parameters β_j are large values that shift lower states to higher energies. The excited states and ground state share the same basis and the same circuit with different variational parameters.

To implement VQD, it is crucial to calculate the wave function overlap $|\langle j|k\rangle|^2$, which is realized by $|\langle 0|U^\dagger(j)U(k)|0\rangle|^2$ [20]. We can prepare the state $U^\dagger(j)U(k)|0\rangle$ using the trial state circuit followed by the inverse of the previously computed state. The overlap is obtained by measuring the final probability of $|\uparrow\uparrow\uparrow\uparrow\rangle$. This method requires the same number of qubits as VQE and at most twice the circuit depth. Note that there are several methods to compute excited states such as the quantum phase estimate method [1,8,31], the quantum Lanczos method [26,32], and the quantum equation of motion [4,33]. VQD has been widely applied in quantum chemistry [34–36]. In addition, VQD requires low resources to compute excited states. In applications of the VQD method, one should be cautious since errors would be accumulated due to the successive solving procedure and become larger for higher states. The detailed analysis of error accumulation in VQD has been discussed in Ref. [20].

III. SYSTEMS AT FINITE TEMPERATURES

A. Seniority model

The exact eigenvalues of the degenerate pairing Hamiltonian with N particles can be obtained by the seniority model as [27]

$$E_N^s = -\frac{G}{4}(N - s)(2\Omega - N - s + 2), \tag{8}$$

where s is the seniority quantum number representing the number of unpaired nucleons.

The eigenstates are usually degenerate except for the ground state. The degeneracy of excited states is related to s as [27]

$$d_s = \binom{\Omega}{s/2} - \binom{\Omega}{s/2 - 1}, \tag{9}$$

while s satisfies $s \leqslant N$. It is consistent with the results of exact diagonalization of pairing Hamiltonian shown in Table I.

The system at a finite temperature kT is described by the canonical ensemble. The partition function can be written as

$$Z_c = \sum_s d_s \exp\left[-\beta\left(E_N^s - E_N^0\right)\right], \tag{10}$$

where $\beta = 1/kT$ and k is the Boltzmann constant. The pairing energy at the finite temperature kT is given by

$$\langle H\rangle = \frac{1}{Z_c}\sum_s d_s E_N^s \exp\left[-\beta\left(E_N^s - E_N^0\right)\right]. \tag{11}$$

B. Finite temperature BCS theory

The finite temperature BCS (FT-BCS) or Bogoliubov theory has been widely used for descriptions of compound nuclei [10]. The partition function is based on quasiparticle excitations. Within the FT-BCS theory, the pairing gap equation is written as [10]

$$\Delta = \Delta_0 \tanh\left(\tfrac{1}{2}\beta\Delta\right), \tag{12}$$

where $\Delta_0 = \frac{G\Omega}{2}$ is the BCS gap at zero temperature. The expectation value of the pairing Hamiltonian is

$$\langle H\rangle_{\mathrm{FT-BCS}} = -G\frac{N^2}{4\Omega} - \frac{\Delta^2}{G}. \tag{13}$$

Within FT-BCS, there is a "phase transition" from a paired state to a normal state at a critical temperature corresponding to $kT_c = \frac{1}{2}\Delta_0$ [10]. The critical temperature is around 0.7 MeV for compound nuclei [16,37].

C. Thermal states by VQE

Thermal excited states are mixed states which can be described by the density matrix

$$\rho_\beta = \frac{1}{Z_c}\sum_i e^{-\beta E_i}|\psi_i\rangle\langle\psi_i|, \tag{14}$$

note that ψ_i is the eigenstate of Hamiltonian. The expectation value of an observable $\hat{O}$ is defined by $\langle\hat{O}\rangle = \mathrm{Tr}(\rho_\beta\hat{O})$. The pairing energy can be calculated by

$$\langle H\rangle = \frac{1}{Z_c}\sum_i e^{-\beta E_i}\langle\psi_i|H|\psi_i\rangle \equiv \langle\psi_c|H|\psi_c\rangle, \tag{15}$$

while $|\psi_c\rangle \equiv \frac{1}{\sqrt{Z_c}}\sum_i e^{-\beta E_i/2}|\psi_i\rangle$. Actually $|\psi_c\rangle$ is not known as *a priori* and is supposed to be determined by VQE. The preparation of thermal equilibrium states with unitary quantum operations is not trivial. It is known that a mixed thermal state can be generated by thermofield double states [38], however, it is difficult to be applied to a general Hamiltonian. Besides, the quantum imaginary time evolution has only been applied to geometric local Hamiltonians for thermal states [32]. The quantum computing of zeros of the partition function is an alternative way to study phase transitions and thermodynamic quantities [39]. In our case, it is possible to construct a superposition of eigenstates without off-diagonal elements to simulate the mixed thermal states.

Based on VQE, the thermal state can be determined by minimizing the free energy F:

$$F = \langle H\rangle - TS. \tag{16}$$

It is easy to calculate the first term $\langle H\rangle$ based on the variational wave function. In regard to a mixed state, which is described by $\rho = \sum_i p_i|\psi_i\rangle\langle\psi_i|$, the definition of its Von Neumann entropy is $-k\sum_i p_i \ln p_i$. The probability p_i is the overlap between $|\psi_i\rangle$ and $|\psi_c\rangle$. The second term of free energy can be expressed as

$$TS = -kT\sum_i |\langle\psi_i|\psi_c\rangle|^2 \ln|\langle\psi_i|\psi_c\rangle|^2, \tag{17}$$

while $|\psi_i\rangle$ are previously computed eigenstates of the pairing Hamiltonian at zero temperature. Finally, the cost function can be written as

$$\langle\psi(\lambda)|F|\psi(\lambda)\rangle = \langle\psi(\lambda)|H|\psi(\lambda)\rangle + kT\sum_i |\langle\psi_i|\psi(\lambda)\rangle|^2 \ln|\langle\psi_i|\psi(\lambda)\rangle|^2, \tag{18}$$

where $\psi(\lambda)$ is the trial wave function of ψ_c. The quantum computing of overlaps is described in the implementation of VQD. The variational parameters are obtained by minimizing the free energy in case eigenvalues are not known or not precise. The variational measurements of $\langle H\rangle$ can be implemented on the same variational circuit without accurate knowledge of eigenstates. The solving procedure at finite temperatures can be summarized as

(1) a circuit to get each state ψ_i (including ground state) using the VQD method;

(2) a VQE circuit to compute $\langle H\rangle$ for ψ_c with varying parameters;

(3) a circuit to compute the overlaps $|\langle\psi_i|\psi_c\rangle|^2$ as described in the VQD method;

(4) an iterative minimization of the cost function of free energies at different temperatures. Note that the error accumulation by the VQD method has no influence in calculations of $\langle H\rangle$, but it would affect the precision of entropy. The precision of entropy relies on the precision of eigenfunctions and their orthogonal properties. In this work, the entropy is calculated with the knowledge of eigenfunctions, and this is not very efficient for large systems. This method can be improved in the future if the entropy can be obtained with more efficient methods by exploiting the advantages of quantum computing.

In practical calculations, the number of variational parameters can be reduced by considering the degeneracy of excited states. For $\Omega = 3$, the eigenspace is three-dimensional, as shown in Table I. To describe the superposition state, we need at least two parameters. Considering the degeneracy, the parameter space can be reduced to one-dimensional, such as $\psi(\alpha) = \cos\alpha|0\rangle + \frac{\sin\alpha}{\sqrt{2}}(|1\rangle + |2\rangle)$. The state preparation circuit for calculating excited states can also be used for thermal states, in which the two variational parameters satisfy the relation

$$\eta = -\frac{\pi}{4} + \arctan\left(\frac{2\cot\alpha - 1}{\sqrt{3}}\right), \tag{19a}$$

$$\theta = 2\arccos\left(\frac{\cos\alpha + \sin\alpha}{\sqrt{3}}\right). \tag{19b}$$

For $\Omega = 4$ and $N = 4$, the eigenspace is six-dimensional as shown in Table I and five variational parameters are needed. By considering the degeneracy, we construct the trial wave function in a two-dimensional parameter space $\{\alpha, \beta\}$, $|\psi\rangle = \cos\alpha|\mathrm{g.s.}\rangle + \frac{\sin\alpha\cos\beta}{\sqrt{3}}\sum_{i=0,1,2}|E_1\rangle_i +$

TABLE II. The solved eigenspace of the pairing Hamiltonian for $\Omega = 3$. This table also lists the eigenvalue of the ground state (g.s.), the first degenerate excited states (1st es) from the Qiskit simulator, raw quantum computing energies from IBM_oslo, the readout error-mitigated energies (R-Miti), the zero-noise extrapolation energies (ZNE), and energies from combined readout error-mitigation and zero-noise extrapolation. See text for details.

Eigenstate	$\|\psi\rangle$	E(Qiskit)	E(IBM_oslo)	E(R-Miti)	E(ZNE)	E(R-Miti+ZNE)
g.s.	$0.588\|\uparrow\uparrow\downarrow\rangle + 0.554\|\uparrow\downarrow\uparrow\rangle + 0.590\|\downarrow\uparrow\uparrow\rangle$	−4.013	−3.751	−3.871	−3.919	−4.123
1st es	$0.309\|\uparrow\uparrow\downarrow\rangle + 0.651\|\uparrow\downarrow\uparrow\rangle - 0.693\|\downarrow\uparrow\uparrow\rangle$	−1.024	−1.126	−1.107	−1.093	−1.064
	$0.809\|\uparrow\uparrow\downarrow\rangle - 0.569\|\uparrow\downarrow\uparrow\rangle - 0.146\|\downarrow\uparrow\uparrow\rangle$	−1.004	−1.109	−1.086	−1.006	−0.978

$\frac{\sin\alpha\sin\beta}{\sqrt{2}}\sum_{j=0,1}|E_2\rangle_j$, in which $|\text{g.s.}\rangle$, $|E_1\rangle_i$ and $|E_2\rangle_j$ are the eigenstates of the ground state, the first, and second excited states, respectively. The two parameters α, β can be related to the rotational parameters in the circuit.

IV. COMPUTING EIGENSTATES

In this work, the quantum simulations are performed on the open platform Qiskit [22]. The practical quantum computations are performed on the superconducting quantum processor IBM_oslo, which has seven qubits. Its median CNOT error is about 8.3×10^{-3} and its median readout error is about 2.2×10^{-2}. In addition to the number of CNOT gates, the structure of the circuit and the architecture of quantum processor could also affect the accuracy. The transpiler can optimize the executing circuit according to the hardware architecture. The calculations used 15000 shots for each measurement.

A. Ω = 3

First the ground state of $\Omega = 3$ with four particles is solved by the quantum simulator. The eigenspace is three-dimensional as shown in Table I. There are two variational parameters η, θ. The expectation value of the Hamiltonian given by the quantum simulator is -4.013, while the the exact value is -4.0. The resulted variational parameters are $\theta = 1.62\pi$, $\eta = 1.26\pi$. The wave function of the ground state is $|gs\rangle_{\text{sim}} = 0.588|\uparrow\uparrow\downarrow\rangle + 0.554|\uparrow\downarrow\uparrow\rangle + 0.590|\downarrow\uparrow\uparrow\rangle$, which is quite close to the exact wave function $0.577(|\uparrow\uparrow\downarrow\rangle + |\uparrow\downarrow\uparrow\rangle + |\downarrow\uparrow\uparrow\rangle)$, as their overlap is 0.9994.

The excited states are simulated with the same circuit as for the ground state. After the wave function of the ground state is obtained, the effective Hamiltonian of excited states is constructed according to Eq. (7). Then excited states are solved by VQD with two variational parameters. Note that the first excited state have a double degeneracy. The two solutions correspond to parameters as $\{1.8\pi, 1.76\pi\}$ and $\{1.4\pi, 0.42\pi\}$, respectively. The resulted excited energies are -1.024 and -1.004, respectively, while the exact value is -1.0. Note that wave functions of degenerate states are not uniquely determined. The degenerate states are solved successively and the second degenerate state is obtained by VQD after the first state is shifted out of the eigenspace via Eq. (7).

Quantum computing of ground state and excited states of $\Omega = 3$ are also displayed in Table II. To compare with the simulation results, the same variational parameters are used in quantum computing. For the ground state, the obtained energy is -3.751 with IBM_oslo, which has a deviation due to the noisy hardware about 6% compared to simulations. The degenerate energies of the first excited states are -1.126 and -1.109, respectively. The quantum-noisy deviations of excited states are about 13% with comparison with simulations. The deviations are mainly come from the noisy CNOT gates and the decoherence in readout measurements.

B. Error mitigation

Next we applied the error mitigation of readout measurements of eigenstates of $\Omega = 3$ with IBM_oslo. The detailed results are listed in Table II. For each qubit, there is a readout error probability of $P(0|1)$ and $P(1|0)$. The measurement error can be mitigated by applying the inverse of the error matrix of kth qubit [6,30]

$$S_k = \begin{pmatrix} P^k_{0,0} & P^k_{0,1} \\ P^k_{1,0} & P^k_{1,1} \end{pmatrix}. \tag{20}$$

Note that such readout error mitigation is performed for individual qubits. The readout error mitigation is demonstrated to be very useful to improve the quantum computing accuracy with a large number of qubits [30]. In our case, the ground state energy after the error mitigation is -3.871, while the raw value is -3.751. The error-mitigated first excited state energies are -1.107 and -1.086, while the raw values are -1.126 and -1.109. We see that the readout error mitigation is significant for the ground state but has minor influences for excited states.

We also applied the zero-noise extrapolation [6] for the error mitigation of CNOT gates. For each measurement on IBM_oslo, we add two and four additional CNOT gates. Note that the product of two CNOT gates is the identity. Based on these results, corresponding to one, three, and five CNOT repetitions, the polynomial fitting can extrapolate the error mitigated results with zero CNOT gate. This procedure of error mitigation has been widely adopted [2,3,6,40]. The higher-order extrapolation with more CNOT repetitions could be too noisy to be helpful. The linear fit is applied to get the error-mitigate results. The ground state energy is -3.305 and -2.664 with two and four additional CNOT gates. The zero-noise extrapolation is -4.015 with four CNOT gates and -3.919 with two CNOT gates. Actually, the output eigenvectors with four additional CNOT gates have serious decoherence. The zero-noise extrapolation for the degenerated excited states with two additional CNOT gates are -1.093 and -1.006, respectively. The zero noise extrapolation method is a phenomenological error mitigation but can improve the accuracy

TABLE III. The eigenvalues of the pairing Hamiltonian for $\Omega = 4$ from practical quantum computing. The readout error-mitigation (R-Miti) and zero-noise extrapolation (ZNE) results are also shown.

Eigenstate	E(Qiskit)	E(IBM_oslo)	E(R-Miti)	E(ZNE)
g.s.	−5.958	−4.534	−4.754	−5.376
1st es	−2.020	−2.108	−2.124	−2.055
	−2.000	−1.963	−1.976	−1.895
	−2.004	−2.071	−2.097	−2.107
2nd es	−0.064	−0.809	−0.728	−0.620
	−0.015	−0.655	−0.559	−0.233

remarkably. The results in Table II show that the combination of the readout error mitigation and zero-noise extrapolation does not improve the accuracy.

C. Ω = 4

The problem of $\Omega = 4$ is much more complex than that of $\Omega = 3$. For $\Omega = 4$ with four particles, the eigenspace is six-dimensional and five variational parameters are needed. In this case, the circuit becomes complicated because we have to realize the entanglement of six basis on four qubits. With five variational parameters, we have to employ classical optimization methods to find the global minima. We have applied the Nelder-Mead method which is a widely used derivative-free optimization method for finding multidimensional global minima [41]. The Nelder-Mead method is based on the transformation of multi-dimensional simplex. Note that the hybrid quantum-classical computation as a promising direction has been extensively studied [4,21,30,42], since quantum computing is only superior on specific tasks. The simulation with Qiskit results in an energy of −5.958 for the ground state, while the exact value is −6.0. Here the deviation is originated from statistical fluctuations and the multidimensional optimization. Similar to $\Omega = 3$, the excited states are solved successively by VQD. The calculated energies of the first degenerate excited state are −2.020, −2.000, −2.004, respectively, while the exact values are −2.0. The energies of the second degenerate excited state are −0.064 and −0.015, respectively, while the exact values are 0.0. It can be seen that accumulated deviations increase for higher states. The overlaps between eigenstates are also checked. The orthogonality is satisfactory and this is crucial for simulations of thermal states.

For quantum computing of $\Omega = 4$ eigenstates, the ground state is maximally entangled and the result of the complex circuit is −4.534. Its deviation is about 24%. The detailed results are shown in Table III. The quantum computing of the first degenerate excited states is rather satisfactory. However, the results of the second degenerate excited states have large deviations, since more computing basis are entangled compared to the first excited states. Note that in the IBM_oslo processor some qubits are not directly connected. The nonlocal operations can result in large noise. For $\Omega = 4$, the readout error mitigation and zero-noise extrapolation have also been performed. We see that results can be much improved by the zero-noise extrapolation. The largest deviation for $\Omega = 4$ after the zero-noise extrapolation is about 0.6, which is much larger than 0.1 for $\Omega = 3$. The circuit in Fig. 2 works for both ground state and excited states of $\Omega = 4$. For testing calculations, we also construct another circuit only for the first excited state on four qubits. The first excited state only involve the superposition of two basis as shown in Table I, so that the circuit is much simpler. The resulted energy with IBM_oslo is -1.97 ± 0.03, while the Qiskit value is −1.993. We see that the reduced eigenspace can greatly improve the accuracy. In Ref. [30], the first excited state of ^{6}Li also employs a simpler circuit and has a more accurate result compared to the ground state considering their different eigenspaces.

V. RESULTS AT FINITE TEMPERATURES

The thermal excitation states can be constructed with the eigenstates provided by zero-temperature calculations. These eigenstates are almost completely orthogonal so that an entanglement state can approximate the mixed thermal state. The exact solutions are given by the seniority model. For comparison, the FT-BCS results which are not suitable for small systems are also shown.

A. Ω = 3

For $\Omega = 3$ with $N = 4$ particles, the Qiskit simulations of pairing energies as a function of temperatures are shown in Fig. 3. The temperature is given in the scale of Δ_0. With the FT-BCS approximation, there is a phase transition around temperature $kT = 0.5\Delta_0$ as expected, which should be smoothed out in finite systems. The BCS ground state energy is −3.55. At high temperatures, the FT-BCS energy is −1.33 which is contributed from the Hartree term and the pairing gap is vanished. We see there is a significant discrepancy between FT-BCS and exact results. The exact energies show a smooth transition as a function of temperatures. The FT-BCS results are higher than exact results both at zero and finite temperatures, since BCS includes insufficient many-body correlations. With increasing temperatures, the pairs are breaking due to thermal excitations. However, the pairs can not be fully broken due to a restricted configuration space. At the limit of high temperatures, the system would have the largest entropy and eigenstates are equally mixed, and the energy limit should be −2.0 rather than −1.33 as given by FT-BCS.

The false phase transition in FT-BCS demonstrates the breakdown of the BCS approximation for small systems. Note that BCS violates the conservation of particle number due to the breaking of U(1) symmetry. The symmetry restoration by particle number projection can improve the FT-BCS results [12]. However, the results of projected FT-BCS at high temperatures are close to FT-BCS [12], which is not consistent with exact results of the seniority model. It is known that FT-BCS with variation after projection can well reproduce the nondegenerate pairing model [43]. The energy discrepancy between exact solutions and FT-BCS at high temperatures demonstrates an analogy existence of a pseudogap pairing [13], i.e., a gap above T_c is needed in Eq. (13) to account for the energy discrepancy. Here, the existence of the pseudogap pairing at high temperatures is due to the symmetry constraint

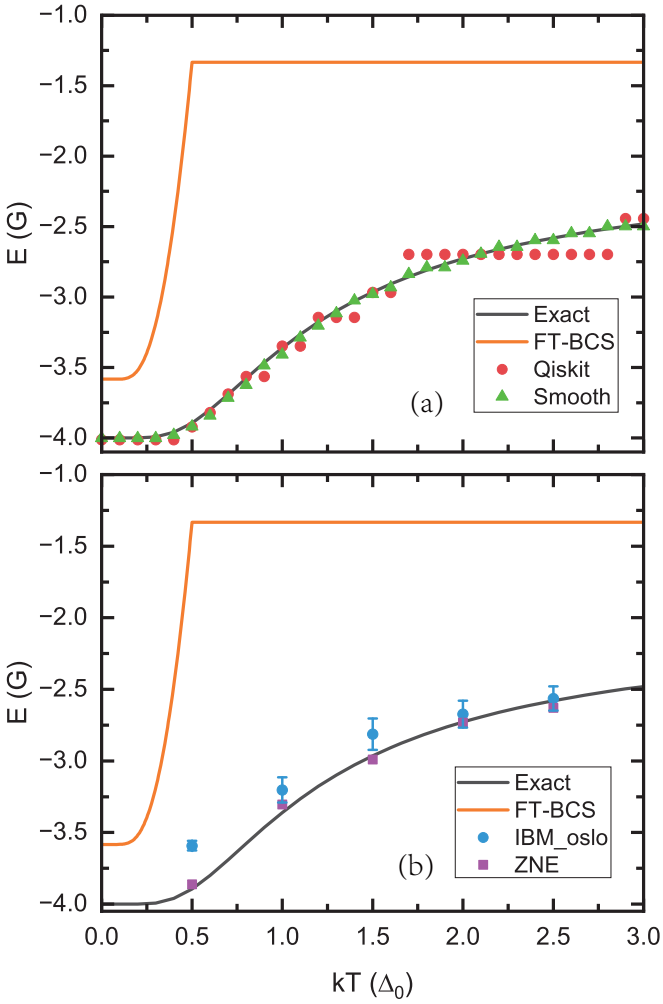

FIG. 3. (a) The pairing energies of $\Omega = 3$ as a function of temperatures obtained from FT-BCS and Qiskit. The original Qiskit and smoothed simulation results are shown. (b) The same pairing energies and zero-noise extrapolation (ZNE) results obtained by quantum computing.

of finite systems. This provides a clue for the origin of the pseudogap phase in high-T_c superconductors which may be induced by specific localized symmetries. The breakdown of FT-BCS and the variation before projection on FT-BCS implies the accurate treatment of many-body correlations in such small thermal-excited systems is essential.

With Qiskit simulations, the deviations caused by statistical fluctuations are much larger at finite temperatures than at zero temperature. This is because the calculation of entropy based on wave function overlaps adds more statistical noise. In Fig. 3, to reduce the noise, only one variational parameter is used considering the degeneracy of the first excited state. The original Qiskit simulations show large deviations from exact values. To this end, we applied numerical smoothing and interpolation to smooth out the statistical fluctuations in variational parameters. Then the smoothed results are close to exact values at finite temperatures. As an example, the variational free energy at $kT = 2.7\Delta_0$ is shown in Fig. 4. We see that the Qiskit simulations have small fluctuations

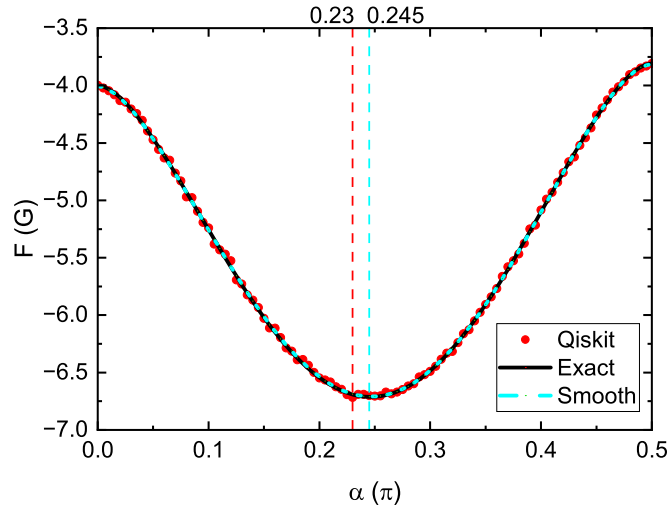

FIG. 4. The simulated free energies of $\Omega = 3$ as a function of variational parameters at the temperature of $kT = 2.7\Delta_0$. The optimized variational parameters from Qiskit simulations and smoothed simulations are shown for comparison.

around exact free energies. This results in small deviations in determining the variational parameter. However, the determination of pairing energies of thermal states is sensitive to these variational parameters. Thus the smoothed VQE is necessary to improve the accuracies of thermal quantum simulations.

The quantum computing results with IBM_oslo are shown in Fig. 3(b). Note that in the quantum computing, the variational parameters are taken from Qiskit simulations to reduce uncertainties. We can see that the quantum computing results are slightly higher than exact values and also demonstrate a smooth phase transition as expected. For each temperature, we made five measurements and the hardware uncertainties given by the standard variances are also shown. The earlier described error mitigation by zero-noise extrapolation is also applied at finite temperatures. The error mitigated results by the zero noise extrapolation become close to exact values.

B. $\Omega = 4$

For $\Omega = 4$, the quantum simulations at finite temperatures are more complex. We adopt two variational parameters

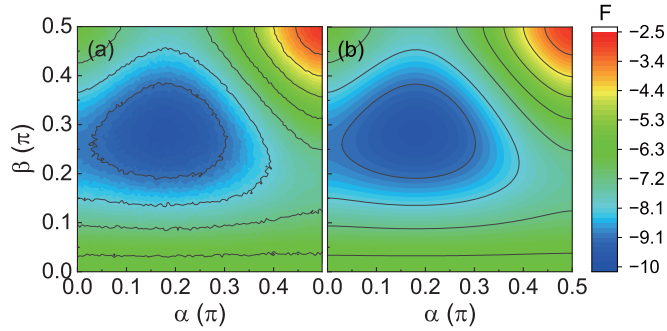

FIG. 5. (a) The contour of free energies with two variational parameters by quantum simulations at $kT = 2.0\Delta_0$ for $\Omega = 4$. (b) The smoothed contour around the minima.

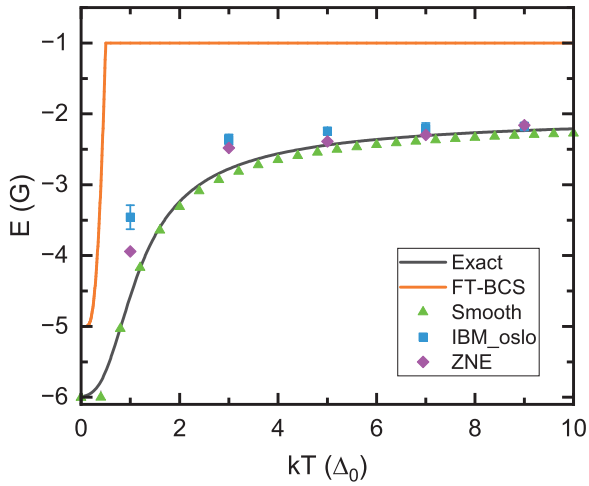

FIG. 6. The pairing energies and the zero-noise extrapolation (ZNE) from quantum computing as a function of temperatures for $\Omega = 4$. The FT-BCS results and exact results are shown for comparison. The smoothed simulation results by Qiskit are also shown.

considering the degeneracy of excited states. In principle there are five variational parameters but the influences of statistical noise would be very large. Figure 5 shows the Qiskit simulations of free energies with two variational parameters. We see notable fluctuations in the contour which would be difficult for VQE to determine precisely the variational parameters. Figure 5(b) shows the smoothed contour with the Fourier expansion. The smoothing method can also be applied to multidimensional parameter spaces.

The thermal excitation energies of the pairing Hamiltonian of $\Omega = 4$ at finite temperatures are shown in Fig. 6. The FT-BCS results are also shown. It is known that the original Qiskit results have notable fluctuations in free energies. The smoothed simulations are necessary to obtain correct variational parameters and thus correct pairing energies. The quantum computing results and zero-noise extrapolation are shown. The zero-noise extrapolation results are satisfactory compared to exact solutions. In general, the quantum computing results of $\Omega = 4$ are less accurate compared to that of $\Omega = 3$. In both cases, the deviations of quantum computing become smaller with increasing temperatures, due to the cancellation between errors of different states. This is promising for quantum computing of thermal states although accumulated errors by VQD increase at higher states. For even larger systems or very high temperatures, a hybrid approach can be used, in which low-lying states are computed by VQD and high-lying states are computed by approximate methods such as the mean-field approximation plus symmetry projections.

VI. CONCLUSION

We performed quantum computing of eigenstates and thermal states of the pairing Hamiltonian in a degenerate shell. For $\Omega = 3$ and $\Omega = 4$ with four particles, we show their wave functions can be simulated on three and four qubits, which correspond to much larger shell model spaces. We have applied VQD for excited states that shifts lower states out of the eigenspace successively. The quantum computing is performed with a superconducting quantum processor provided by IBM. The error mitigation of readout measurements and the zero-noise extrapolation have been demonstrated to be helpful to improve the accuracy. For $\Omega = 4$, the entanglement of six basis on four qubits is realized and the circuit is constructed using the two-qubit building blocks that preserve the number of particles.

The mixed thermal state is simulated by the entanglement of the orthogonal eigenspace with the same variational circuit as at zero temperature. For comparison, the finite-temperature BCS results are also shown, which has a false phase transition from superfluid state to normal state. The quantum computing demonstrates a smooth transition as expected in finite systems. The FT-BCS is breakdown for small systems. In addition, exact results are not close to FT-BCS at high temperatures, indicating an analogy existence of pairing pseudogap. In our approach, the thermal excitations can be simulated without accurate knowledge of eigenvalues. The results from quantum computing become close to exact solutions at high temperatures. In the future, it is still desirable to develop an improved quantum algorithm to compute the entropy more efficiently. The accurate treatment of many-body correlations of finite thermal systems has broad physics implications, for which quantum computing has unique opportunities.

ACKNOWLEDGMENTS

We are grateful for discussions with F. R. Xu. This work was supported by the National Key R&D Program of China (Contract No. 2018YFA0404403) and by the National Natural Science Foundation of China under Grants No. 11975032, No. 11835001, No. 11790325, and No. 11961141003. We acknowledge the use of IBM Q cloud and the Qiskit software package.

[1] D. S. Abrams and S. Lloyd, Phys. Rev. Lett. **83**, 5162 (1999).
[2] E. F. Dumitrescu, A. J. McCaskey, G. Hagen, G. R. Jansen, T. D. Morris, T. Papenbrock, R. C. Pooser, D. J. Dean, and P. Lougovski, Phys. Rev. Lett. **120**, 210501 (2018).
[3] M. J. Cervia, A. B. Balantekin, S. N. Coppersmith, C. W. Johnson, P. J. Love, C. Poole, K. Robbins, and M. Saffman, Phys. Rev. C **104**, 024305 (2021).
[4] M. Q. Hlatshwayo, Y. N. Zhang, H. Wibowo, R. LaRose, D. Lacroix, and E. Litvinova, Phys. Rev. C **106**, 024319 (2022).
[5] B. Hall, A. Roggero, A. Baroni, and J. Carlson, Phys. Rev. D **104**, 063009 (2021).
[6] A. Roggero, C. Y. Gu, A. Baroni, and T. Papenbrock, Phys. Rev. C **102**, 064624 (2020).
[7] W. Du, J. P. Vary, X. Zhao, and W. Zuo, Phys. Rev. A **104**, 012611 (2021).
[8] D. Lacroix, Phys. Rev. Lett. **125**, 230502 (2020).
[9] P. Lv, S. Wei, H.-N. Xie, and G. Long, Sci. China Phys. Mech. Astron. **66**, 240311 (2023).

[10] A. L. Goodman, Nucl. Phys. A **352**, 30 (1981).
[11] Y. Alhassid, C. N. Gilbreth, and G. F. Bertsch, Phys. Rev. Lett. **113**, 262503 (2014).
[12] C. Esebbag and J. L. Egido, Nucl. Phys. A **552**, 205 (1993).
[13] P. Magierski, G. Wlazłowski, and A. Bulgac, Phys. Rev. Lett. **107**, 145304 (2011).
[14] T. Timusk and B. Statt, Rep. Prog. Phys. **62**, 61 (1999).
[15] P. Fanto, Y. Alhassid, and G. F. Bertsch, Phys. Rev. C **96**, 014305 (2017).
[16] V. Martin, J. L. Egido, and L. M. Robledo, Phys. Rev. C **68**, 034327 (2003).
[17] J. C. Pei, W. Nazarewicz, J. A. Sheikh, and A. K. Kerman, Phys. Rev. Lett. **102**, 192501 (2009).
[18] H. Shen, F. Ji, J. N. Hu, and K. Sumiyoshi, Astrophys. J. **891**, 148 (2020).
[19] A. Peruzzo, J. McClean, P. Shadbolt, M.-H. Yung, X.-Q. Zhou, P. J. Love, A. Aspuru-Guzik, and J. L. OBrien, Nat. Commun. **5**, 4213 (2014).
[20] O. Higgott, D. Wang, and S. Brierley, Quantum **3**, 156 (2019).
[21] J. R. McClean, J. Romero, R. Babbush, and A. Aspuru-Guzik, New J. Phys. **18**, 023023 (2016).
[22] IBM, Qiskit: An Open-source Framework for Quantum Computing, https://qiskit.org/.
[23] P. Jordan and E. Wigner, Z. Phys. **47**, 631 (1928).
[24] E. Ovrum and M. Hjorth-Jensen, arXiv:0705.1928v1.
[25] A. Khamoshi, F. A. Evangelista, and G. E. Scuseria, Quantum Sci. Technol. **6**, 014004 (2021).
[26] E. A. Ruiz Guzman and D. Lacroix, Phys. Rev. C **105**, 024324 (2022).
[27] P. Ring and P. Schuck, *The Nuclear Many-Body Problem* (Springer, New York, 2004).
[28] P. K. Barkoutsos, J. F. Gonthier, I. Sokolov, N. Moll, G. Salis, A. Fuhrer, M. Ganzhorn, D. J. Egger, M. Troyer, A. Mezzacapo, S. Filipp, and I. Tavernelli, Phys. Rev. A **98**, 022322 (2018).
[29] B. T. Gard, L. Zhu, G. S. Barron, N. J. Mayhall, S. E. Economou, and E. Barnes, NPJ Quantum Inf. **6**, 10 (2020).
[30] O. Kiss, M. Grossi, P. Lougovski, F. Sanchez, S. Vallecorsa, and T. Papenbrock, Phys. Rev. C **106**, 034325 (2022).
[31] A. Aspuru-Guzik, A. D. Dutoi, P. J. Love, and M. Head-Gordon, Science **309**, 1704 (2005).
[32] M. Motta, C. Sun, A. T. K. Tan, M. J. O'Rourke, E. Ye, A. J. Minnich, F. G. S. L. Brandao, and G. K.-L. Chan, Nat. Phys. **16**, 205 (2020).
[33] P. J. Ollitrault, A. Kandala, C.-F. Chen, P. K. Barkoutsos, A. Mezzacapo, M. Pistoia, S. Sheldon, S. Woerner, J. M. Gambetta, and I. Tavernelli, Phys. Rev. Res. **2**, 043140 (2020).
[34] Y. Ibe, Y. O. Nakagawa, N. Earnest, T. Yamamoto, K. Mitarai, Q. Gao, and T. Kobayashi, Phys. Rev. Res. **4**, 013173 (2022).
[35] Q. Gao, G. O. Jones, M. Motta, M. Sugawara, H. C. Watanabe, T. Kobayashi, E. Watanabe, Y. y. Ohnishi, H. Nakamura, and N. Yamamoto, NPJ Comput. Mater. **7**, 70 (2021).
[36] J. W. Wen, D. S. Lv, M.-H. Yung, and G.-L. Long, Quantum Eng. **3**, e80 (2021).
[37] E. Khan, N. Van Giai, and N. Sandulescu, Nucl. Phys. A **789**, 94 (2007).
[38] J. Wu and T. H. Hsieh, Phys. Rev. Lett. **123**, 220502 (2019).
[39] A. Francis, D. Zhu, C. H. Alderete, S. Johri, X. Xiao, J. K. Freericks, C. Monroe, N. M. Linke, and A. F. Kemper, Sci. Adv. **7**, eabf2447 (2021).
[40] I. Stetcu, A. Baroni, and J. Carlson, Phys. Rev. C **105**, 064308 (2022).
[41] W. H. Press, S. A. Teukolsky, W. T. Vetterling, and B. P. Flannery, *Numerical Recipes* (Cambridge University Press, Cambridge, 2007).
[42] N. Klco, E. F. Dumitrescu, A. J. McCaskey, T. D. Morris, R. C. Pooser, M. Sanz, E. Solano, P. Lougovski, and M. J. Savage, Phys. Rev. A **98**, 032331 (2018).
[43] D. Gambacurta and D. Lacroix, Phys. Rev. C **85**, 044321 (2012).